Source process of the September 12, 2007 M_W 8.4 Southern Sumatra earthquake from tsunami tide gauge record inversion

Stefano Lorito, Fabrizio Romano, Alessio Piatanesi and Enzo Boschi

Istituto Nazionale di Geofisica e Vulcanologia, Via di Vigna Murata 605, 00143 Rome, Italy

Abstract

We infer the slip distribution and average rupture velocity of the magnitude M_W 8.4 September 12, 2007, Southern Sumatra earthquake from available tide-gauge records of the ensuing tsunami. We select 9 waveforms recorded along the west coast of Sumatra and in the Indian Ocean. We assume the fault plane and the slip direction to be consistent with both the geometry of the subducting plate and the early focal mechanism solutions. Slip distribution and rupture velocity are determined simultaneously by means of a non linear inversion method. We find high slip values (~10 m) into a patch 100 km long and 50 km large, between 20 and 30 km of depth, about 100 km north-west from the epicenter. Our estimate of rupture velocity is of 2.1±0.4 km/sec. The relatively large depth of the main slip patch is the likely explanation for the small observed tsunami.

1. Introduction

On September 12, 2007 at 11:10:26 UTC an earthquake of magnitude M_W 8.4 occurred off the west coast of Sumatra about 130 km SW of Bengkulu. The epicenter was localized at 4.517°S and 101.382°E, between the Sunda trench and Bengkulu (Figure 1). The induced sea-floor displacement generated a moderate tsunami that nevertheless propagated through the Indian Ocean and was recorded for example also by the tide-gauge at Salalah, Oman. Apart from minor aftershocks, it was followed, 12 hours later, by another earthquake of magnitude M_W 7.9 near the Sumatra coast, 185 km SSE of Padang (Figure 1). Both earthquakes caused in total 25 fatalities and 161 people were injured [ref. USGS]. The seismic sequence continued on the next two days, with the biggest event of magnitude M_W 7.1 happening on September 13. This sequence took place in the same zone where the historical earthquakes of 1797 and 1833 also generated significant tsunamis [*Nalbant et al.,* 2005].

This is the fourth very large earthquake to occur on the Sunda megathrust and generating a significant tsunami in less than three years (Figure 1). We recall the huge Sumatra-Andaman earthquake and tsunami of December 26, 2004 with a magnitude M_W 9.2 and a rupture extent of almost 1,300 km, that caused widespread victims and destruction on the Indian Ocean coasts. The Sumatra-Andaman 2004 event was followed later on by the M_W 8.7 earthquake and tsunami of Simeulue-Nias (March 28, 2005), generated along the Sunda trench on the stretch just contiguous to the Southern end of the Sumatra-Andaman 2004 rupture zone. The imminence of the Nias earthquake was predicted as a consequence of the coseismic stress induced by the slip distribution of the Sumatra-Andaman earthquake [*McCloskey et al.,* 2005]. The rupture zone of the Simeulue-Nias earthquake has also a significant overlap with that of the historical 1861 earthquake and tsunami [*Nalbant et al.,* 2005]. The next destructive tsunami earthquake was the M_W 7.7 Java event (July 17, 2006), with a rupture zone displaced southward with respect to the one of the Simeulue-Nias event. It generated an abnormally large tsunami with respect to what expected by its

seismically radiated energy and it has been then catalogued as a "tsunami earthquake" [*Ammon et al.*, 2006; *Fuji and Satake*, 2006].

The inversion of tsunami waveforms is an important tool for characterizing the seismic source of off-shore earthquakes. Recently, such inversions have been performed by *Piatanesi and Lorito* (2007) and by *Fuji and Satake* (2007) to characterize the kinematic rupture of the 2004 Sumatra-Andaman earthquake.

A better understanding of the rupture process of tsunamigenic earthquakes originating on the Sunda megathrust is in turn a key issue for evaluating the possible consequences of future events both for the risk mitigation and the warning strategies design [*Borrero et al.,* 2006; *Geist et al.,* 2007*; McCloskey et al.*, 2007a; *McCloskey et al.*, 2007b].

Here we perform the inversion of the waveforms recorded by 9 tide-gauge stations distributed in the Indian Ocean both in the near and in the far field with respect to the source zone. Our goal is to retrieve the slip distribution and the average rupture velocity of the September 12, 2007 earthquake.

2. Sea-level Data

The tsunami waves generated by the September 12, 2007 earthquake were recorded by tide-gauge stations distributed in the Indian Ocean in the shallow waters of harbors and coastal sites. The data were available for download in near real time at the website of the University of Hawaii Sea Level Center (UHSLC; http://ilikai.soest.hawaii.edu/RSL/). Most of these stations are operated by the Global Sea Level Observing System (GLOSS; http://www.gloss-sealevel.org/).

The tsunami was also recorded by the DART buoy 23401 in the deep ocean northwest of Sumatra. This buoy is owned and operated by the Thailand Meteorological Department (TMD) in conjunction with National Disaster Warning Center of the Kingdom of Thailand. Data were available in real-time at the National Data Buoy Center (NDBC) website (http://www.ndbc.noaa.gov/dart.shtml), maintained by the U.S. National Oceanic and Atmospheric Administration (NOAA).

77 Both the UHSLC and the DART 23401 records of this tsunami have a sampling rate of one minute.
78 The positions of the stations we choose for the inversion are plotted on the map of Figure 1. Before
79 using these data in the inversion, we remove tidal components to extract the tsunami signal and we
80 select only the first cycles of the waveforms that are less sensitive to local bathymetry than later
81 arrivals. We use an even narrow time window for Padang and Sibolga stations since they clearly
82 show a resonant character in the later phases.
83
84 **3. Seismic Source Parameters**
85 To define the dimension of the causative fault, we use the spatial distribution of the aftershocks
86 occurred during 12 hours after the mainshock, that is available at the National Earthquake
87 Information Center website of the U.S. Geological Survey (USGS;
88 http://neic.usgs.gov/neis/epic/epic.html). We choose a region large enough to contain all the
89 aftershocks, and then we end up with a length of 350 km and a width of 200 km (Figure 2).
90 The strike of the source is 323° roughly parallel to the Sunda trench [*Bird,* 2003]. The dip is fixed at
91 12°, using the quick moment tensor solution of the Global CMT project. We adopt a slip direction
92 (rake) of 105°, basing both on the focal mechanism and on the finite fault model calculated by C. Ji
93 according to the algorithm described in *Ji et al.* [2002], and available at
94 http://www.geol.ucsb.edu/faculty/ji/big_earthquakes/2007/09/sumatra_seismic.html/.
95 We split the source region into 28 square subfaults of dimension 50x50 km (see Table 1 of the
96 Online Supplementary Material). The slip amount on each subfault is to be determined as a result of
97 the inversion, along with the average rupture velocity.
98
99 **4. Tsunami Modeling and Bathymetric Dataset**
100 For each of the subfaults we calculate the corresponding marigrams at the coordinates of the tide-
101 gauges, which are the Green's functions we will use for the inversion.

The initial seawater elevation is assumed to be equal to the coseismic vertical displacement of the sea bottom corresponding to an assumed "unitary" slip of 3 meters [*Piatanesi and Lorito*, 2007], and computed through the Okada's analytical formulas [*Okada*, 1992], while the initial velocity field is assumed to be identically zero. The boundary conditions are pure wave reflection at the solid boundary (coastlines) and full wave transmission at the open boundary (open sea). The tsunami wave propagation from the initial field to the tide-gauges is calculated by solving the non linear shallow water equations, including Coriolis force and bottom friction, with a finite differences scheme on a staggered grid. More detailed description of the equations as well as of the numerical method can be found in *Lorito et al.* [2008], *Piatanesi and Lorito* [2007] and *Mader* [2001].

The computational domain is shown in Figure 1. We choose a grid resolution for tsunami propagation of 1 arc-minute. The bathymetry grid is obtained by merging different bathymetric datasets [e.g. *Geist et al.*, 2007; *Fujii and Satake*, 2007]. We use as a background the 1 arc-min GEBCO bathymetry *[British Oceanographic Data Center*, 2003], version 1.02, available at the British Oceanographic Data Center website (http://www.bodc.ac.uk/data/online_delivery/gebco/). To improve the bathymetry in shallow waters, particularly along the coast of Sumatra and around some of the tide-gauges, we digitize, where available to us, 9 nautical charts *(United Kingdom Hydrographic Office*, 2005; see Figure 1). We then remove the shallow water points from GEBCO in correspondence of the digitized dataset and interpolate both on local 0.5 arc-min subgrids, before resampling to 1 arc-min and merging to the whole domain.

5. Inversion

We use a non linear inversion method based on the simulated annealing technique to simultaneously infer both slip distribution and average rupture velocity, with a L1-L2 hybrid norm as cost function. The details can be found in *Piatanesi and Lorito* [2007] and in *Lorito et al.* [2008], and in the references therein.

The average rupture velocity is assumed to be the uniform velocity of a circular front propagating out from the hypocenter on the fault plane. We consequently add the appropriate delay to the Green's function corresponding to each subfault, according to their distance along the rupture path. The resolving power of the inversion setup (azimuthal coverage, sampling rate, fault parametrization, etc.) is tested by means of a checkerboard experiment, with target slip values of alternatively 2 and 6 meters on adjacent subfaults. We first tune the subfaults size by means of several checkerboard experiments, starting with larger sizes and ending up with 50 by 50 km. We moreover test for different rupture velocities. The synthetic waveforms generated with the checkerboard slip distribution are corrupted with Gaussian noise, with a variance that is 20% of the clean time series variance. We let the slip range between 0 and 15 meters, at 1 meter steps, whilst the velocity ranges between 0.5 and 3.5 km/sec, at 0.5 km/sec steps.

The target slip distribution, i.e. the checkerboard pattern, is reproduced fairly well by the best model (Figure 2, and Table 1 of the Online Supplementary Material), with a root mean square of the differences between target and inverted values of 0.8 meters. Conversely, the target rupture velocity of 2.5 km/sec is not inferred exactly, as our best model estimation is 2 km/sec. Following *Piatanesi and Lorito* [2007], we estimate the uncertainty of each inverted parameters through an appraisal of the ensemble of the models explored during the search stage (see Table 1 of the Online Supplementary Material). In particular, the marginal distribution of the explored velocity values shows quite a broad peak ranging between 2 and 2.5 km/sec (see inset of Fig. 2). The average model estimation of the rupture velocity is 2.2±0.3 km/sec, that is consistent with the target velocity of 2.5 km/sec. Later, in the real case inversion, we will then assume the average model value, in place of the best model, as our estimate of the rupture velocity.

The checkerboard experiment results indicate that the dataset has the capability of resolving the main features of the rupture kinematics, with a good resolution for the slip and a relatively worst resolution for the velocity.

153 To retrieve the rupture features of the September 12, 2007 earthquake, we adopt the same subfaults
154 geometry and parameter ranges as in the checkerboard experiments. Moreover we adjust of a few
155 minutes the arrival times of the Green's functions at the stations of Cocos, Sibolga, Colombo,
156 Diego Garcia and Pointe La Rue, at which we observed systematic differences between recorded
157 and simulated phases. *Arcas and Titov* [2006] discussed the difficulty in reproducing coastal in
158 comparison to offshore propagation, due to the poor bathymetry knowledge along with the
159 contamination from unmodeled coastal processes. We actually use the GEBCO bathymetry only at
160 some of the stations and did not simulate inundation, likely leading to travel times inaccuracy. An
161 adjustment of travel times has been performed also by *Fuji and Satake* [2006], who observed
162 discrepancies at the Cocos station while studying the 2006 Java tsunami. In the present case,
163 however, we verified that the inverted rupture velocity is only slightly dependent on such arrival
164 time adjustments.
165 The slip distribution of the best model we find is shown in Figure 3. According to our results, the
166 rupture propagated with a velocity of 2.1±0.4 km/sec, with a relatively low slip (2 to 3 meters)
167 around the hypocentral zone. The rupture then propagated to the North-West featuring the highest
168 slip concentration (up to 12 meters) at about 3-3.5°S and 101°E, at a depth ranging between 20 to
169 30 km. We notice that this main patch is surrounded by most of the aftershocks. We also plot the
170 resulting coseismic vertical displacement, to be compared with the geodetic data when available.
171 The whole set of results, best model and average model with associated errors is reported in Table 1
172 in the online supplementary material. The best model slip values always fall well inside the error
173 bars. Conversely, the best model velocity lies at the upper edge of the error bar, confirming the best
174 model is an extreme one in this context and as velocity is concerned.
175 The match between the recorded and inverted waveforms is generally good (Figure 4). In some of
176 the cases, as those of Padang (the nearest station to the source) and the DART buoy (the most
177 reliable data) is excellent. The worst case is Diego Garcia, with at least the period well reproduced,

178 while missing its amplitude. Overall, we satisfactorily reproduce the main features of the September
179 12, 2007 tsunami wave amplitudes and periods, and, in some cases, the arrival times.
180
181 **6. Conclusions**
182 We find that the source of the September 12, 2007 Southern Sumatra earthquake has been
183 characterized by its highest slip values (~10 m) concentrated into a patch 100 km long and 50 km
184 large, located between 20 and 30 km of depth, about 100 km north-west from the epicenter. The
185 occurrence of such a slip amount has been suggested by *Nalbant et al.* [2005], who indicated that
186 the greatest current seismic threat from the Sunda megathrust may came from a section overlapped
187 with the source of the September 12, 2007 earthquake, with a slip as great as in 1833: that is, up to
188 10 meters.
189 The slip release has been very low or even absent at depths lower than 10-15 km. A shallower slip
190 patch of about 2-3 meters occurred only around the epicentral latitudes.
191 These results are in fair agreement, at least as regard the localization of the main slip patches, with
192 those of Chen Ji
193 (http://www.geol.ucsb.edu/faculty/ji/big_earthquakes/2007/09/sumatra_seismic.html/), and in a
194 lesser extent with those of Yuji Yagi (http://www.geo.tsukuba.ac.jp/press_HP/yagi/EQ/20070912/).
195 Nevertheless, the above teleseismic inversions infer a much lower slip amount than our inversion of
196 tsunami waveforms.
197 Our best model features a seismic moment of 4.8×10^{21} N·m, if we use a shear modulus $\mu=6.0 \times$
198 10^{10} N/m^2 [*Geist and Bilek*, 2001], corresponding to a magnitude M_W 8.39 earthquake. This result is
199 consistent with the USGS estimation of a M_W 8.4 earthquake magnitude.
200 The depth of the earthquake is an important factor in controlling the tsunami amplitude especially in
201 the near field. On one hand, slip at depth produces relatively small vertical displacement of the sea
202 bottom. On the other hand, high slip at intermediate depths on the megathrust produces maximum
203 sea floor displacements in shallow waters thus generating tsunamis with relatively small potential

204 energy. The absence of significant slip at shallow depths is then a likely explanation for the
205 generation of a relatively moderate tsunami. As a comparison, the tsunami generated by the smaller
206 and shallower Java 2006 M_W 7.7 earthquake was by far more destructive, and it has been then
207 catalogued as a "tsunami earthquake" [*Fuji and Satake*, 2006].
208
209 **Acknowledgments.** We gratefully acknowledge the contribution of Alessio Mautone, at the INGV
210 SISMOS laboratory, who scanned the nautical charts we used in this work.
211 Some figures have been produced with Generic Mapping Tools software (Wessel and Smith, 1998).
212
213 **References**
214 Ammon, C. J., H. Kanamori, T. Lay and A. A. Velasco (2006). The 17 July 2006 Java tsunami
215 earthquake, *Geophys. Res. Lett.*, *33*, L24308, doi:10.1029/2006GL028005.
216 Arcas, D., and V. V. Titov (2006), Sumatra tsunami: lessons from modeling, *Surv. Geophys.*, *27*,
217 679-705, doi:10.1007/s10712-006-9012-5.
218 Bird, P. (2003), An updated digital model of plate boundaries, *Geochem. Geophys. Geosystems*, *4*,
219 1027, doi:10.1029/2001GC000252.
220 Borrero, J.C., K. Sieh, M. Chlieh, and C. E. Synolakis (2006), Tsunami inundation modeling for
221 western Sumatra, *Proc. Nat. Acad. Sci.*, *103*, 19673-19677.
222 British Oceanographic Data Center (2003). *The Centenary Edition of the GEBCO Digital Atlas*
223 [CD-ROM], Liverpool, UK.
224 Fujii Y., and K. Satake (2006), Source of the July 2006 West Java tsunami estimated from tide
225 gauge records, *Geophys. Res. Lett.*, *33*, L24317, doi:10.1029/2006GL028049.
226 Fujii Y., and K. Satake (2007), Tsunami Source of the 2004 Sumatra–Andaman Earthquake
227 Inferred from Tide Gauge and Satellite Data, *Bull. Seismol. Soc. Am.*, *97*, S192–S207,
228 doi:10.1785/0120050613.

229 Geist, E.L., and S. L. Bilek (2001), Effect of depth-dependent shear modulus on tsunami generation
230 along subduction zones, *Geophys. Res. Lett.*, *28*, 1315-1318.
231 Geist, E.L., V.V. Titov, D. Arcas, F. F. Pollitz, and S. L. Bilek (2007), Implications of the 26
232 December Sumatra-Andaman earthquake on tsunami forecast and assessment models for
233 great subduction-zone earthquakes, *Bull. Seismol. Soc. Am.*, *97*, S249-S270, doi:
234 10.1785/0120050619.
235 Ji, C., D.J. Wald, and D.V. Helmberger (2002), Source description of the 1999 Hector Mine,
236 California earthquake; Part I: Wavelet domain inversion theory and resolution analysis,
237 *Bull. Seism. Soc. Am.*, *92*, 1192-1207.
238 Lorito, S., A. Piatanesi, and A. Lomax (2008), Rupture Process of the 18 April 1906 California
239 Earthquake from Near-Field Tsunami Waveform Inversion, *Bull. Seismol. Soc. Am.*, in
240 press.
241 Mader, C. L. (2001). *Numerical modeling of water waves*, Los Alamos series in Basic and Applied
242 Sciences, 206 p.
243 McCloskey J., S. S. Nalbant, and S. Steacy (2005), Indonesian earthquake Earthquake risk from co-
244 seismic stress, *Nature*, *434*, 291 – 291.
245 McCloskey, J., A. Antonioli, A. Piatanesi, K. Sieh, S. Steacy, S.S. Nalbant, M. Cocco, C. Giunchi,
246 J.D. Huang, and P. Dunlop (2007a), Near-field propagation of tsunamis from megathrust
247 earthquakes, *Geophys. Res. Lett.*, *34*, L14316, doi:10.1029/2007GL030494.
248 McCloskey, J., A. Antonioli, A. Piatanesi, K. Sieh, S. Steacy, S.S. Nalbant, M. Cocco, C. Giunchi,
249 J.D. Huang, and P. Dunlop (2007b), Tsunami Threat in the Indian Ocean from a Future
250 Megathrust Earthquake West of Sumatra, *Earth Planet. Sci. Lett.*, in press.
251 Nalbant S. S., S. Steacy, K. Sieh, D. Natawidjaja, and J. McCloskey (2005), Seismology:
252 Earthquake risk on the Sunda trench, *Nature*, *435*, 756-757, doi:10.1038/nature435756a.
253 Okada, Y. (1992), Internal deformation due to shear and tensile faults in a half-space, *Bull. Seismol.*
254 *Soc. Am.*, *82*, 1018-1040.

255 Piatanesi, A., and S. Lorito (2007), Rupture process of the 2004 Sumatra-Andaman earthquake
256 from tsunami waveform inversion, *Bull. Seismol. Soc. Am.*, *97*, 223-231,
257 doi:10.1785/0120050627.
258 United Kingdom Hydrographic Office (2005). Catalogue of Admiralty Charts and Publications,
259 2005 Edition, Taunton, Somerset, United Kingdom.
260 Wessel, P., and W. H. F. Smith (1998), New, improved version of the Generic Mapping Tools
261 Released, EOS Trans. AGU, 79, 579.
262

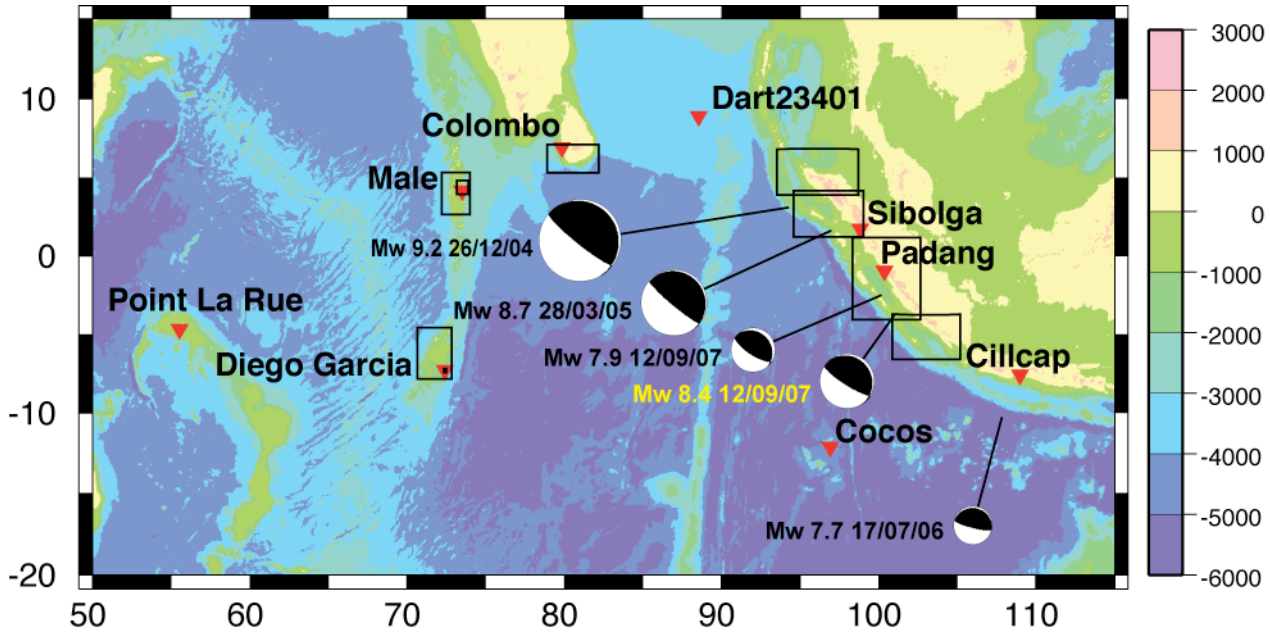

Figure 1. Epicenter and focal mechanism of the M_W 8.4 earthquake of 12 September 2007, along with the epicentral positions and focal mechanisms of the major recent tsunamigenic earthquakes on the Sunda trench. The triangles indicate the positions of the tide-gauge stations and of the DART buoy 23401. The bathymetry used for the simulation is represented by the colorscale. The rectangles are the limits of the nautical charts digitized to construct the bathymetric dataset.

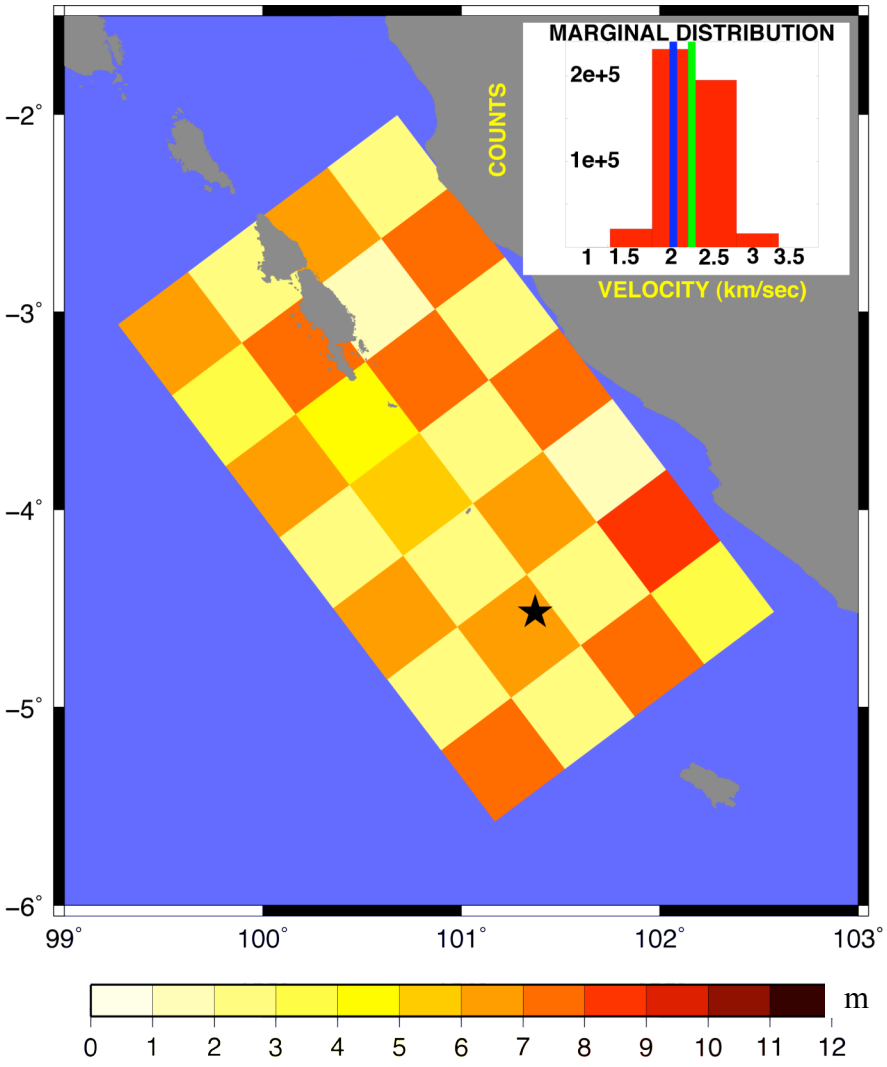

Figure 2. Slip distribution of the best model resulting from the checkerboard test: the rectangles represent the projection of the subfaults to the Earth's surface. The black star indicates the epicenter position. The inset shows the marginal distribution of the rupture velocity; the blue and green vertical solid lines represent the best and average model value respectively.

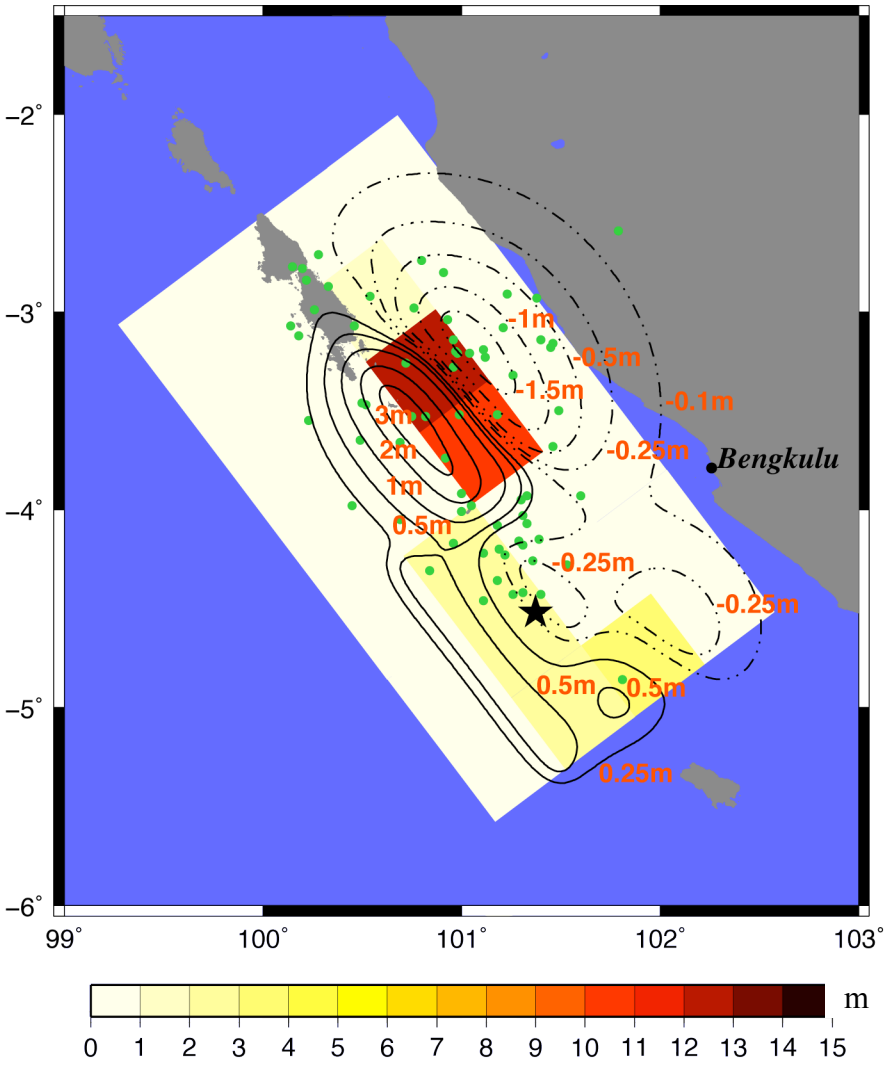

277

278

279 **Figure 3**. Slip distribution of the best model resulting from the September 12, 2007 Sumatra event;

280 rectangles represent the projection of the subfaults to Earth's surface. The black star indicates the

281 epicenter of the mainshock and the green circles are the epicenter of the aftershocks occurred 12

282 hours after the main event. Solid and dashed contour lines represent the positive and negative

283 vertical displacement respectively.

284

285

286

287

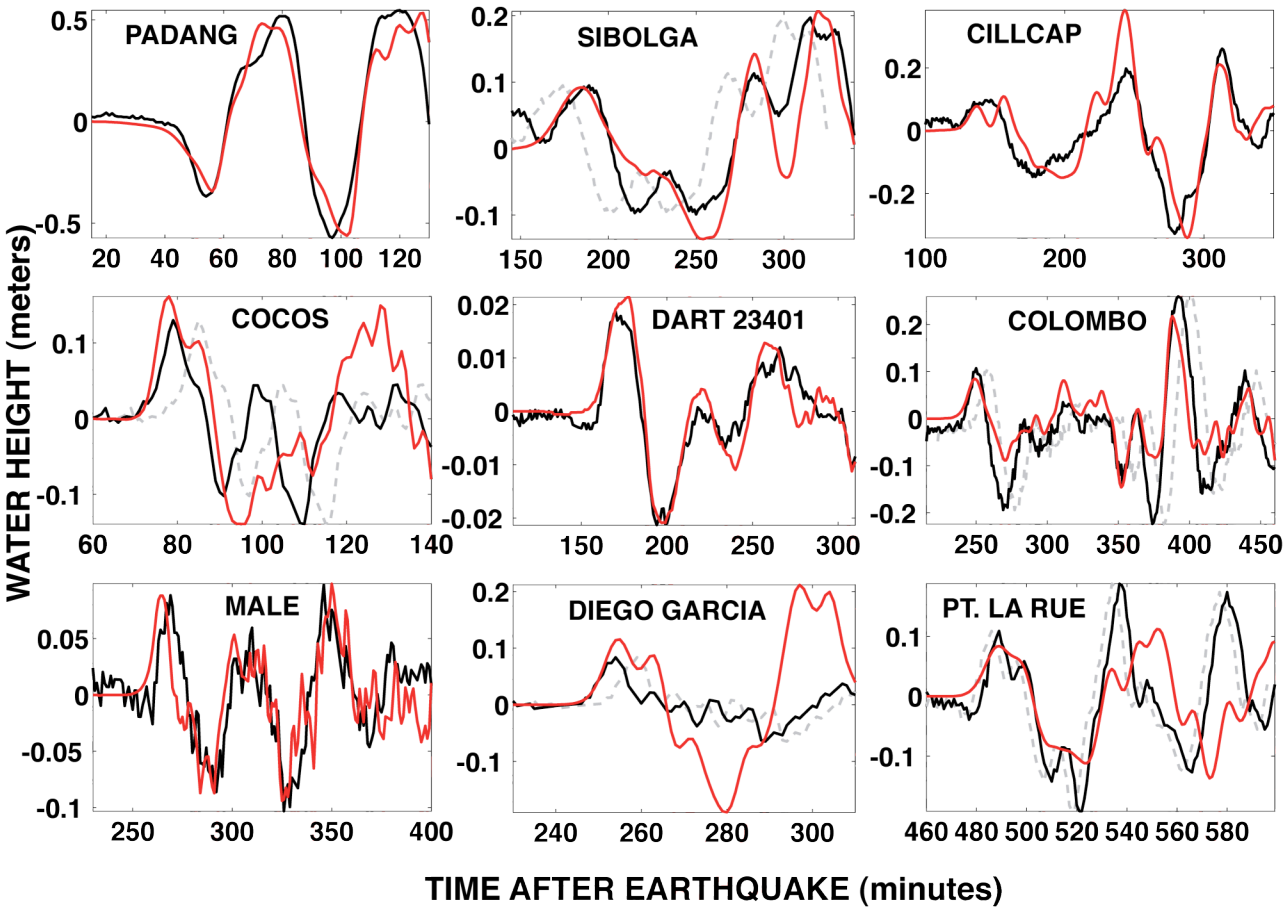

Figure 4. Comparison between the observed time-shifted records (black solid lines) and computed waveforms using the inverted best model (red solid lines). Grey dashed lines are the original observed records.